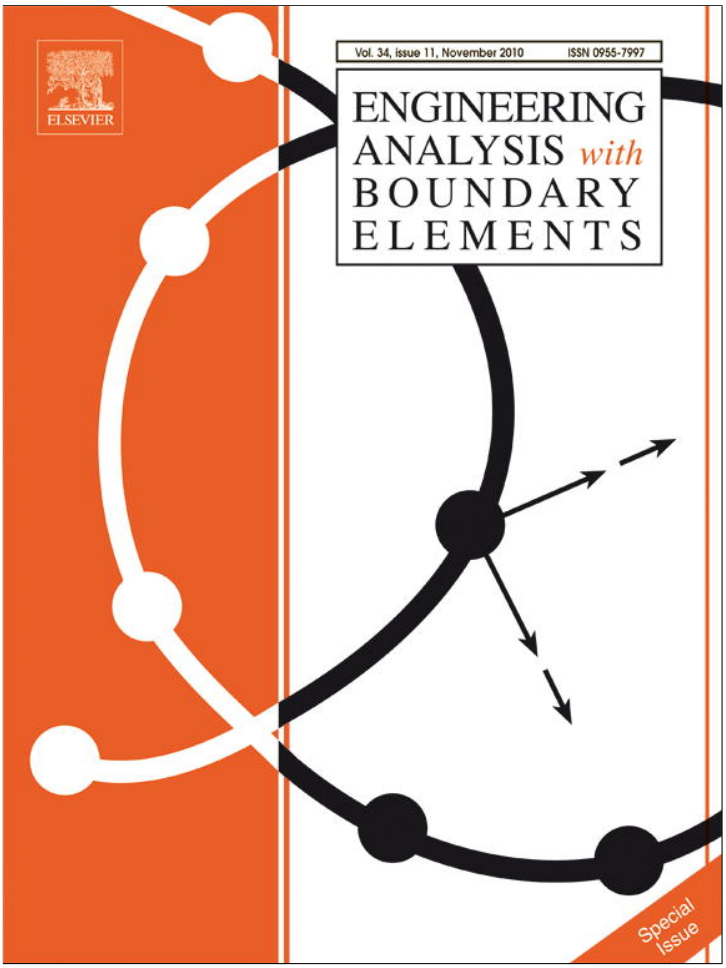

Engineering Analysis with Boundary Elements 34 (2010) 963–970

Contents lists available at ScienceDirect

Engineering Analysis with Boundary Elements

journal homepage: www.elsevier.com/locate/enganabound

Transient analysis of the DSIFs and dynamic *T*-stress for particulate composite materials—Numerical vs. experimental results

V. Guduru [a], A.-V. Phan [a,*], H.V. Tippur [b]

[a] Department of Mechanical Engineering, University of South Alabama, Mobile, AL 36688, USA
[b] Department of Mechanical Engineering, Auburn University, Auburn, AL 36849, USA

ARTICLE INFO

Article history:
Received 16 February 2010
Accepted 18 April 2010

Keywords:
Dynamic stress intensity factors
Dynamic *T*-stress
Symmetric-Galerkin boundary element method

ABSTRACT

The fracture behavior of particulate composite materials when subjected to dynamic loading has been a great concern for many industrial applications as these materials are particularly susceptible to impact loading conditions. As a result, many numerical and experimental techniques have been developed to deal with this class of problems. In this work, the fracture behavior of particulate composites under impact loading conditions is numerically studied via the two most important fracture parameters: dynamic stress intensity factors (DSIFs) and dynamic *T*-stress (DTS), and the results are compared with the experimental data obtained in Refs. [1,2]. Here, micromechanics models (self-consistent, Mori–Tanaka, …) or experimental techniques need to be employed first to determine the effective material properties of particulate composites. Then, the symmetric-Galerkin boundary element method for elastodynamics in the Fourier-space frequency domain is used in conjunction with displacement correlation technique to evaluate the DSIFs and stress correlation technique to determine the DTS. To obtain transient responses of the fracture parameters, fast Fourier transform (FFT) and inverse FFT are subsequently used to convert the DSIFs and DTS from the frequency domain to the time domain. Test examples involving free–free beams made of particulate composites are considered in this study. The numerical results are found to agree very well with the experimental ones.

1. Introduction

Composite materials are particularly susceptible to impact loading conditions in which loads are applied rapidly, randomly or deliberately such as those seen in aerospace, automotive, production, or construction industries, etc. As a result, it is important to understand the fracture behavior of composite materials under these loading conditions. Conventional theories suggest that the fracture behavior can be assumed by the crack initiation, propagation and branching in the vicinity of a crack tip. The two important fracture parameters which can be used to describe the dynamic fracture behavior are the dynamic stress intensity factors (DSIFs) and dynamic *T*-stress (DTS). Therefore, many numerical and experimental techniques have been developed to study these parameters.

To determine the DSIFs and DTS experimentally, one needs to measure the crack tip deformations during a dynamic fracture event at high spatial and temporal resolutions. In the past the focus has been primarily with the accurate evaluation of the former although a few reports have addressed DTS measurements in recent years. The works which have focused on DSIF measurements include those of Dally [3] who used photoelasticity and high-speed photography. Tippur and co-workers [4–7] have used coherent gradient sensing (CGS) method to study the dynamic fracture behavior of a variety of composite materials. Kokaly et al. [8] have used moiré interferometry along with high-speed photography to study aluminum alloys.

The recent advances in high-speed digital imaging at recording rates exceeding a million frames per second has made it feasible to study fast-fracture events using other methods and improve the accuracy of measured fracture parameters. Recently, Kirugulige and co-workers [1] used the method of digital image correlation (DIC) and high-speed photography for the measurement of transient deformations near a crack under dynamic loading. In their work, random speckle patterns on a specimen surface before and after deformation are acquired, digitized and stored. In the undeformed image, subimages are chosen and the locations of similar subimages are identified on the deformed image. Once the subimages are found in the deformed image, the displacements can be easily estimated. The obtained displacements are processed using least-squares method to extract the DSIFs and DTS using asymptotic crack tip field expressions. The measurement of these fracture parameters are shown to favorably compare with their finite element analysis results. Moving from the photographic methods, Jiang et al. [9] used split-Hopkinson pressure bar apparatus to find the dynamic

* Corresponding author. Tel.: +1 251 460 7453; fax: +1 251 460 6549.
E-mail address: vphan@jaguar1.usouthal.edu (A.-V. Phan).

0955-7997/$ - see front matter © 2010 Elsevier Ltd. All rights reserved.
doi:10.1016/j.enganabound.2010.04.010

responses in a pre-cracked specimen. They derived simple formula to find the DSIFs from dynamic responses using vibration analysis method. Ivanyts'kyi et al. [10] applied dynamic torsion on a cylindrical specimen with an external circular crack and proposed a combined numerical and experimental method to determine the DSIFs. Due to the significant influence of the *T*-stress on crack path and crack growth direction, more and more experimental methods devoted to the measurement of this parameter can be found in the literature. For example, Maleski et al. [11] measured the *T*-stress under both static and dynamic loading conditions by optimal positioning of stacked strain gage rosette near a mode-I crack tip.

On the numerical modeling side, several numerical methods have been developed to determine the DSIFs such as finite difference method (FDM, e.g., [12]), finite element method (FEM, e.g., [13]), boundary element method (BEM, e.g., [14]), symmetric-Galerkin boundary element method (SGBEM, e.g., [15,16]) and scaled boundary finite element method (SBFEM, e.g., [17]). In Ref. [15], boundary integral equations (BIEs) for elastodynamics in the frequency domain are employed in conjunction with a modified quarter-point crack-tip element and displacement correlation technique (DCT) to accurately calculate the DSIFs. A conversion of the frequency DSIFs to those in the time domain is done by using fast Fourier transform (FFT) and inverse FFT (IFFT) as described in Ref. [16]. Numerous numerical methods such as FEM (e.g., [18]), BEM (e.g., [19]), SGBEM (e.g., [20,21]), and SBFEM (e.g., [22]) have also been used for determining the *T*-stress, while SBFEM (e.g., [22]), SGBEM (e.g., [23]), and BEM (e.g., [24]) for the DTS. Phan [21] developed a non-singular boundary integral formulation based upon a stress correlation technique for evaluating the *T*-stress and the technique is extended to cover the DTS in Ref. [23]. Song and Vrcelj [22] extended the SBFEM to evaluate the DSIFs and DTS for two dimensional problems without any requirement of internal mesh and asymptotic solution close to the singular point. Sladek et al. [24] used BEM to express path independent integral (*M*-integral) formulation through the dynamic *J*-integrals for determining the DTS on the basis of relation found between the *M*-integral and *T*-stress. A comparison was conducted to the DTS values computed by the *M*-integral, boundary layer and displacement field methods for a rectangular plate with a central crack.

BEM have been recognized as an effective technique for fracture analysis (e.g., [25]). The key feature of the BEM is that only the boundary of the domain is discretized. This implies that, for fracture analysis, the singular stress field ahead of the crack is not approximated, and that remeshing a propagating crack is an easier task. Among the variants of the BEM, SGBEM (e.g., [26]) has several additional advantages: (a) its coefficient matrix is symmetric as the name implies; (b) the use of both displacement and traction BIEs enables fracture problems to be solved without artificial sub-domains; and (c) unlike most variants of the BEM, standard continuous elements can be employed. Thus, SGBEM can easily exploit highly effective quarter-point quadratic elements (e.g., [27]) to accurately capture the crack tip behavior.

In addition to important developments of the SGBEM for stress and fracture analysis in elastostatics, the SGBEM for elastodynamics in the Fourier-space frequency domain has recently been extended to fracture applications [15,16,24]. Following an SGBEM fracture analysis in the frequency domain, FFT and IFFT are subsequently employed to convert the DSIFs and DTS from the frequency domain to the time domain. These transient responses, especially in the immediate aftermath of an impact loading, are of special interest as most dynamic responses usually reach their maximum value during this period.

In this work, the SGBEM for elastodynamics in the Fourier-space frequency domain developed in Refs. [15,16,24] is employed to evaluate the DSIFs and DTS for free–free beams made of particulate composite materials. To this end, the effective material properties ultrasonically measured are utilized. These numerical solutions are compared with some known experimental results for the purpose of validation.

2. Fracture analysis using SGBEM

In this section, fracture analysis using the SGBEM for 2-D elastodynamics in the Fourier-space frequency domain is briefly presented. More details of the technique can be found in, e.g., [16].

Consider a domain of boundary Γ containing a crack. Let $\Gamma=\Gamma_b\cup\Gamma_c^+\cup\Gamma_c^-$ where Γ_b is the boundary of the non-crack part, and Γ_c^+ and Γ_c^- are the "plus" and "minus" surfaces of the crack, respectively. Further, let $\Gamma_b=\Gamma_{bu}\cup\Gamma_{bt}$ where Γ_{bu} and Γ_{bt} are the boundary parts where displacement and traction are known, respectively. Finally, let $\Gamma_t=\Gamma_{bt}\cup\Gamma_c^+$ and note that traction is assumed to be known on the crack surfaces.

For a given angular frequency ω and a source point P interior to a 2-D domain of boundary Γ, the displacement BIE for elastodynamics in the frequency domain is given by

$$\mathcal{U}(P,\omega)\equiv u_k(P,\omega)-\int_{\Gamma_b}\left[U_{kj}(P,Q,\omega)t_j(Q,\omega)-T_{kj}(P,Q,\omega)u_j(Q,\omega)\right]dQ+\int_{\Gamma_c^+}T_{kj}(P,Q,\omega)\Delta u_j(Q,\omega)dQ=0 \tag{1}$$

where Q denotes a field point, U_{kj} and T_{kj} are the elastodynamic kernel tensors (e.g., [28] or [16]), u_j and t_j are the displacement and traction vectors, respectively, and Δu_j is the crack displacement jump vector.

When P is off the boundary, U_{kj} and T_{kj} are not singular and it is possible to differentiate Eq. (1) with respect to P, resulting in the displacement gradients. By substituting these gradients into Hooke's law and then Cauchy's relation, one gets the following traction BIE:

$$\mathcal{T}(P,\omega)\equiv t_k(P,\omega)-n_l(P)\int_{\Gamma_b}\left[D_{kjl}(P,Q,\omega)t_j(Q,\omega)-S_{kjl}(P,Q,\omega)u_j(Q,\omega)\right]dQ+n_l^+(P)\int_{\Gamma_c^+}S_{kjl}(P,Q,\omega)\Delta u_j(Q,\omega)=0 \tag{2}$$

where n_l is the outward normal vector to the boundary and the elastodynamic kernel tensors D_{kjl} and S_{kjl} can also be found in [28] or [16]. This traction equation is required for dealing with crack geometries.

It is known that the limits of the integrals in Eqs. (1) and (2) exist as P approaches Γ. From now on, for a boundary source point P, the displacement and traction BIEs are understood in this limiting sense.

Unlike the collocation methods, the Galerkin approaches enforce Eqs. (1) and (2) over the entire boundary. To obtain a symmetric coefficient matrix as the name SGBEM implies, Eq. (1) needs to be enforced over Γ_{bu} while Eq. (2) is enforced over Γ_t. This is done by using the shape function ψ_m, employed in approximating the boundary tractions and displacements, as weighting functions for these equations

$$\int_{\Gamma_{bu}}\psi_m(P)\mathcal{U}(P,\omega)dP=0 \tag{3}$$

$$\int_{\Gamma_t}\psi_m(P)\mathcal{T}(P,\omega)dP=0 \tag{4}$$

The main computational task in numerically implementing Eqs. (3) and (4) is the evaluation of their singular integrals.

As these equations have a similar form as those in elastostatics, it is convenient to employ a technique based upon the following kernel decomposition:

$$\iint I^d dQdP = \iint I^s dQdP + \iint (I^d - I^s) dQdP \tag{5}$$

where I^d and I^s denote an elastodynamic kernel and its elastostatic counterpart, respectively. On the right-hand side of Eq. (5), treatments for the elastostatic integral $\iint I^s dQdP$ are known elsewhere, while an evaluation of the second integral, which is weakly singular at most, was discussed in, e.g., [16].

3. DSIFs by the SGBEM and displacement correlation technique

Among the methods available for numerically evaluating the DSIFs, the DCT is one of the simplest. For an angular frequency ω, the DSIFs are given by

$$K_{\mathrm{I}}(\omega) = \beta\mu\sqrt{2\pi}\lim_{r\to 0}\frac{\Delta u_n(\omega)}{\sqrt{r}} \tag{6}$$

$$K_{\mathrm{II}}(\omega) = \beta\mu\sqrt{2\pi}\lim_{r\to 0}\frac{\Delta u_t(\omega)}{\sqrt{r}} \tag{7}$$

where Δu_n and Δu_t are the normal and tangential components of the displacement jump vector, respectively, and r is the distance to the crack tip.

In Eqs. (6) and (7),

$$\beta = \frac{4\beta_p\beta_s - (1+\beta_s^2)^2}{4\beta_p(1-\beta_s^2)} \tag{8}$$

and

$$\beta_p = \sqrt{1-(c/c_p)^2} \tag{9}$$

$$\beta_s = \sqrt{1-(c/c_s)^2} \tag{10}$$

$$c_p^2 = \frac{\lambda+2\mu}{\rho} \tag{11}$$

$$c_s^2 = \mu/\rho \tag{12}$$

where ρ is the mass density, c is the crack tip velocity, c_p and c_s are the compressional and shear velocities, respectively, and λ and μ are effective Lamé's constants. For particulate composites, these effective constants can be measured experimentally or determined using micromechanics models such as self-consistent or Mori–Tanaka model (e.g., [29]). Note for elastodynamic analysis that the internal damping of the material can be considered by means of a complex shear modulus defined as

$$\mu_c = \mu(1+2i\zeta) \tag{13}$$

where i is the imaginary unit and ζ is the damping ratio.

The DSIF calculations reported in this work are carried out using the modified quarter point (MQP) element developed in Ref. [27]. By using the MQP shape functions in Eqs. (6) and (7), the mode-I and mode-II DSIFs can be obtained as follows:

$$K_{\mathrm{I}}(\omega) = \frac{\beta\mu}{3}\sqrt{\frac{2\pi}{L}}\left[8\Delta u_n^{(2)} - \Delta u_n^{(3)}\right] \tag{14}$$

$$K_{\mathrm{II}}(\omega) = \frac{\beta\mu}{3}\sqrt{\frac{2\pi}{L}}\left[8\Delta u_t^{(2)} - \Delta u_t^{(3)}\right] \tag{15}$$

where L is the distance between the two end-nodes of the crack tip element, and the superscripts (2) and (3) denote the quarter-point node and the non-crack-tip end-node, respectively.

According to Eqs. (14) and (15), the DSIFs are directly given in terms of the nodal values of the displacement jump of the crack-tip element. As the MQP element enhances the accuracy of the nodal displacement jumps obtained from a SGBEM analysis, the use of the MQP directly improves the accuracy of the obtained DSIFs.

4. DTS by the SGBEM and stress correlation technique

T-stress is a non-singular stress, which is the first non-singular term in the series expansion of the stress component parallel to the crack and ahead of a crack tip. In addition to the SIFs, the T-stress has also been considered as an important fracture parameter as numerous studies have shown that the sign and magnitude of the T-stress can have a substantial influence on the crack tip behavior. For a good review on the roles of the T-stress on different fracture aspects, the reader is referred to the work by Wang [30].

The stress distribution near a crack tip was early investigated by Williams [31]. In polar coordinates (r, θ) associated with this crack tip (see Fig. 1), the stress components σ_{ij} can be expressed by

$$\begin{bmatrix}\sigma_{11} & \sigma_{12}\\ \sigma_{21} & \sigma_{22}\end{bmatrix} = \frac{K_{\mathrm{I}}}{\sqrt{2\pi r}}\begin{bmatrix}f_{11}(\theta) & f_{12}(\theta)\\ f_{12}(\theta) & f_{22}(\theta)\end{bmatrix} + \frac{K_{\mathrm{II}}}{\sqrt{2\pi r}}\begin{bmatrix}g_{11}(\theta) & g_{12}(\theta)\\ g_{12}(\theta) & g_{22}(\theta)\end{bmatrix} + \begin{bmatrix}T & 0\\ 0 & 0\end{bmatrix} + O(r^{1/2}) \tag{16}$$

where the first two terms in the above equation are singular at the crack tip while the third term for σ_{11}, which is parallel to the crack, is finite. This finite term, denoted as T, is the so-called T-stress. Also in Eq. (16), $f_{ij}(\theta)$ and $g_{ij}(\theta)$ are universal functions representing the angular distributions of the crack tip stresses [31].

In the following, the stress correlation technique (SCT) is used to determine the T-stress. By using the expressions for $f_{ij}(\theta)$ and $g_{ij}(\theta)$, Eq. (16) can be explicitly expressed in vector format as follows:

$$\begin{Bmatrix}\sigma_{11}\\ \sigma_{22}\\ \sigma_{12}\end{Bmatrix} = \frac{K_{\mathrm{I}}}{\sqrt{2\pi r}}\cos\frac{\theta}{2}\begin{Bmatrix}1-\sin\frac{\theta}{2}\sin\frac{3\theta}{2}\\ 1+\sin\frac{\theta}{2}\sin\frac{3\theta}{2}\\ \sin\frac{\theta}{2}\cos\frac{3\theta}{2}\end{Bmatrix} + \frac{K_{\mathrm{II}}}{\sqrt{2\pi r}}\begin{Bmatrix}-\sin\frac{\theta}{2}\left(2+\cos\frac{\theta}{2}\cos\frac{3\theta}{2}\right)\\ \sin\frac{\theta}{2}\cos\frac{\theta}{2}\cos\frac{3\theta}{2}\\ \cos\frac{\theta}{2}\left(1-\sin\frac{\theta}{2}\sin\frac{3\theta}{2}\right)\end{Bmatrix} + \begin{Bmatrix}T\\ 0\\ 0\end{Bmatrix} + O(r^{1/2}) \tag{17}$$

For $\theta = 0$ (along the crack direction and ahead of the crack tip)

$$\begin{Bmatrix}\sigma_{11}\\ \sigma_{22}\end{Bmatrix} = \frac{K_{\mathrm{I}}}{\sqrt{2\pi r}}\begin{Bmatrix}1\\ 1\end{Bmatrix} + \begin{Bmatrix}T\\ 0\end{Bmatrix} + O(r^{1/2}) \tag{18}$$

Thus

$$T = \lim_{r\to 0}[\sigma_{11}(r,0) - \sigma_{22}(r,0)] \tag{19}$$

In this work, Eq. (19) is evaluated using the BIE for the stress components. Consider a crack in a finite domain as shown in Fig. 1. Let P be the crack tip and P' be a point ahead of P and in the x_1-direction ($\theta = 0$). The boundary integral representation of the stress components in Eq. (19) involves a limit process in which P'

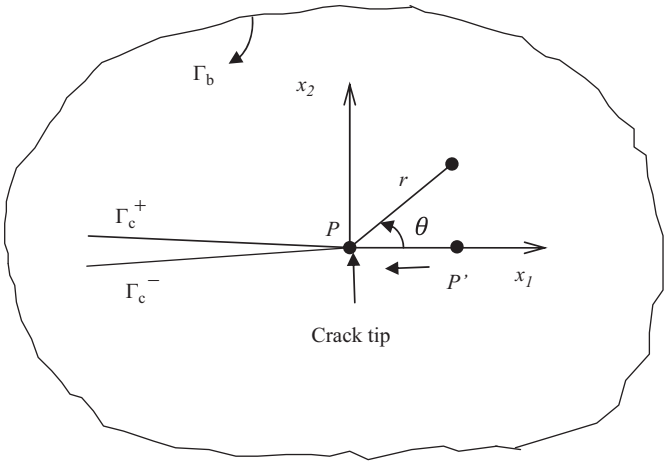

Fig. 1. Crack tip P and crack tip coordinate system x_1–x_2.

tends to the crack tip $P(r\to 0)$ and is given by [21]

$$\sigma_{kl}(P)=\int_{\Gamma_b}\left[D_{klj}(P,Q)t_j(Q)-S_{klj}(P,Q)u_j(Q)\right]dQ - \lim_{P'\to P}\int_{\Gamma_c^+} S_{klj}(P',Q)\Delta u_j(Q)dQ \tag{20}$$

Note that, as the crack surfaces are symmetrically loaded, $\Sigma t_j = t_j^+ + t_j^- = 0$ and thus the integrand term $-D_{klj}(P',Q)\Sigma t_j(Q)$ does not appear in the second integral.

For frequency-domain dynamic fracture analysis, the DTS for an angular frequency ω can be obtained by applying the Fourier transform to Eq. (19). The result is

$$T(\omega)=\lim_{r\to 0}[\sigma_{11}(r,0,\omega)-\sigma_{22}(r,0,\omega)] \tag{21}$$

Substituting the frequency-domain elastodynamic version of Eq. (20) in Eq. (21) results in [23]

$$T(\omega)=\int_{\Gamma_b}\left[\Delta D_j(P,Q,\omega)t_j(Q,\omega)+\Delta S_j(P,Q,\omega)u_j(Q,\omega)\right]dQ + \lim_{P'\to P}\int_{\Gamma_c^+}\left[\Delta S_j(P',Q,\omega)\Delta u_j(Q,\omega)\right]dQ \tag{22}$$

where $\Delta D_j = D_{11j}-D_{22j}$ and $\Delta S_j = S_{22j}-S_{11j}$.

For all $\omega>0$ and as $P'\to P$, the second integral in Eq. (22) must be bounded as T-stress is a finite term. In order to demonstrate that, let rewrite Eq. (22) as follows:

$$T(\omega)=\int_{\Gamma_b}\left[\Delta D_j(P,Q,\omega)t_j(Q,\omega)+\Delta S_j(P,Q,\omega)u_j(Q,\omega)\right]dQ + \lim_{P'\to P}\int_{\Gamma_c^+}\left[\Delta S_j^s(P',Q)\Delta u_j(Q)\right]dQ + \lim_{P'\to P}\int_{\Gamma_c^+}\left[\Delta S_j(P',Q,\omega)-\Delta S_j^s(P',Q)\right]\Delta u_j(Q,\omega)dQ \tag{23}$$

where ΔS_j^s is the static counterpart of ΔS_j.

After this equation being discretized, the only limits required are those associated with the crack tip element. By denoting these limits as T_{ct} one gets

$$T_{ct}=\lim_{P'\to P}\int_{\Gamma_{ct}^+}\Delta S_j(P',Q)\Delta u_j(Q)dQ + \lim_{P'\to P}\int_{\Gamma_{ct}^+}\left[\Delta S_j(P',Q,\omega)-\Delta S_j^s(P',Q)\right]\Delta u_j(Q,\omega)dQ \tag{24}$$

where Γ_{ct}^+ is part of Γ_c^+ discretized by the crack tip element.

By using the standard quadratic shape functions to numerically implement Eq. (24), it can be shown that the first integral in this equation is continuous as $P'\to P$ [21]. The second integral should also be bounded as its integrand is only weakly singular [23]. As a result, the limit processes in Eq. (24) are not necessary and the two integrals can be directly evaluated at the crack tip ($P'\equiv P$).

Here, $T(\omega)$ given by Eq. (23) is evaluated as a post-processing step after t_j, u_j, and Δu_j in this equation are available from the processing stage of a SGBEM dynamic analysis. It can be observed that using Eq. (23) to evaluate the DTS is much simpler and more economic than using other techniques such as the interaction integral method (IIM) (e.g., [24]). As shown in Ref. [23], this technique also offers better accuracy for the DTS than the IIM.

5. Obtaining transient responses from frequency-domain results

For the dynamic analysis of a system in the frequency domain, the dynamic response F (output, such as DSIFs or DTS) of the system and the load P (input) are related by

$$F(\omega)=H(\omega)P(\omega) \tag{25}$$

where $H(\omega)$ is called the frequency response. Since $H(\omega)=F(\omega)/P(\omega)$, the frequency response is the response of the system due to a unit harmonic load $P(\omega)=e^{i\omega t}$.

Fig. 2 depicts a model for obtaining the time history (transient response) from frequency response analysis of damped systems such as those considered in this paper. In this model, the problem under a unit harmonic load ($e^{i\omega t}$) is analyzed first using the SGBEM to obtain the frequency response $H(\omega)$. In the mean time, the time-dependent load $P(t)$ is converted to the frequency domain ($P(\omega)$) by means of FFT. Relation (25) is then employed to obtain the dynamic response $F(\omega)$ in the frequency domain. Finally, IFFT is used to transform $F(\omega)$ into the time domain $F(t)$.

A procedure for obtaining the transient responses by FFT and IFFT can be summarized as follows:

(a) Determine a frequency resolution Δf ($\omega=2\pi f$) which needs to be small enough to minimize the loss of frequency information.
(b) Perform a SGBEM analysis for a series of frequencies, namely $f=0$, Δf, $2\Delta f$, …, $(N/2)\Delta f=f_{\text{Nyq}}$, where $N=2^m$ and m is a positive integer, to obtain the frequency response $H(\omega)$ for the first $(N/2+1)$ samples. Here, the Nyquist frequency f_{Nyq} needs to be chosen such that frequency responses above f_{Nyq} are not significant and can thus be discarded. Note that the very first sample ($k=1$) is the static sample ($f=0$).
(c) For the last $(N/2-1)$ samples ($k=N/2+2$, …, N), $H(\omega)$ must be determined such that it is conjugate symmetric about the Nyquist frequency (see Fig. 3 for an example where $f_{\text{Nyq}}=1.024$ MHz), i.e.,

$$H(k)=\text{conj}(H(N-k+2))(k=N/2+2,\ldots,N) \tag{26}$$

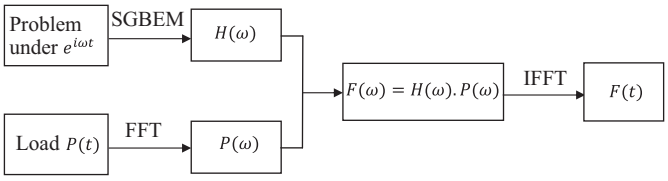

Fig. 2. A model for obtaining the transient responses using FFT and IFFT.

(d) Perform FFT for the time-dependent load $P(t)$ for the N samples ($k=1, \ldots, N$);
(e) Calculate $F(\omega)=H(\omega)P(\omega)$;
(f) Perform IFFT for $F(\omega)$ to obtain the transient response $F(t)$. Note that the period and time resolution (sampling interval) of this transient response are $T_f=1/\Delta f$ and $\Delta t=T_f/N$, respectively;
(g) If the calculated Δt does not provide a good resolution for the shape of the transient curves, interpolation [32] can be used to improve this resolution. This is done by increasing the value of Nyquist's frequency while requiring no extra SGBEM analysis as extra zeros are added to the frequency response (see Fig. 4 where the Nyquist frequency is doubled from 1.024 to 2.048 MHz). As a result, the number of samples N is increased accordingly which enhances the resolution of the transient curves.

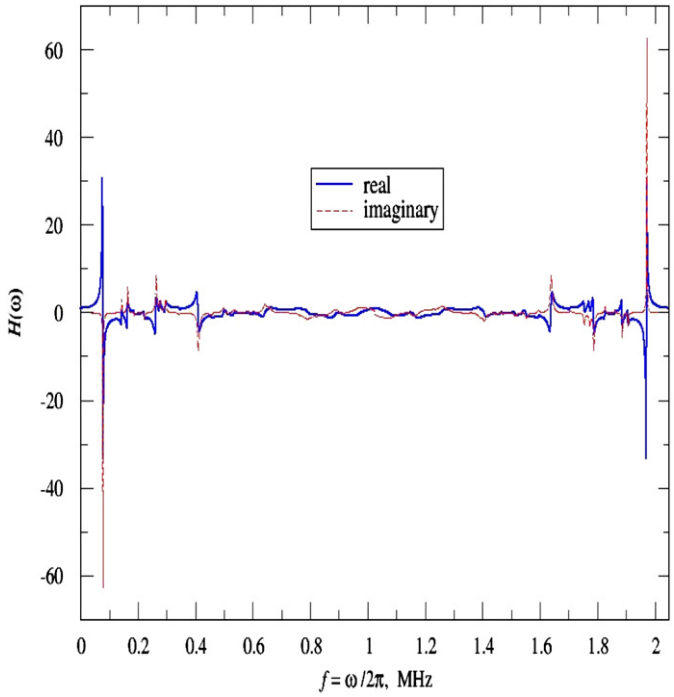

Fig. 3. Conjugate symmetry about Nyquist's frequency of frequency response $H(\omega)$.

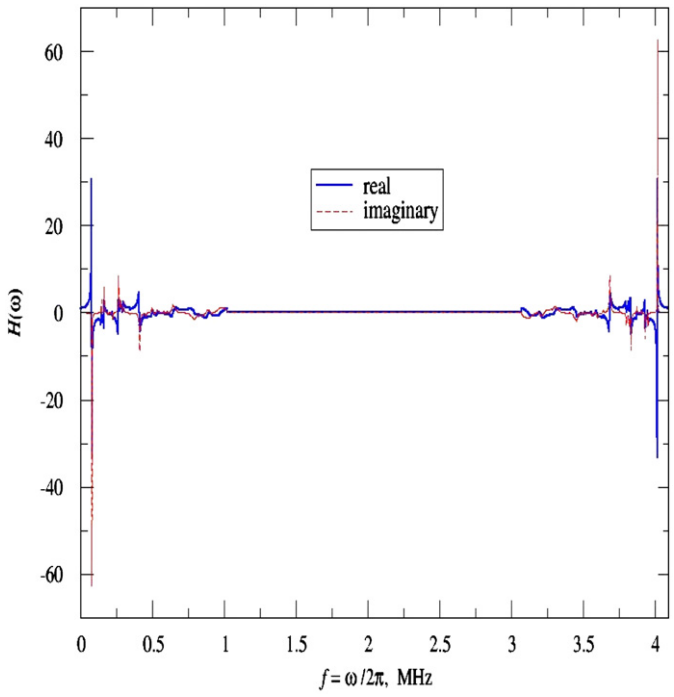

Fig. 4. Doubling time resolution by doubling Nyquist's frequency.

More details on this frequency domain analysis can be found in, e.g., [17] where studies on the effects of the frequency resolution Δf and Nyquist's frequency f_{Nyq} on the computational cost of the analysis were presented.

6. Test problems

For the validation purpose of the proposed numerical techniques discussed in the previous sections, two dynamic fracture problems with known experimental results reported in Refs. [1,2] are selected. These problems involve the mode-I [1] and mixed-mode [2] dynamic fracture of three-point bend beams. As the subject of dynamic crack propagation is beyond the scope of the present work, the validation here is limited to the time instants before crack initiation. According to Refs. [1,2] the crack initiation occurred before a noticeable impact force on the supported anvils (see, e.g., Figs. 5 and 6) because of greater time lag in wave propagation. As the supports do not play any role in the dynamic analysis of the DSIFs and DTS before the crack initiation, instead of three-point bend beams, free–free beams are employed in the numerical simulations presented herein.

As mentioned earlier, the beam geometry, size, materials and loading conditions are adopted from Refs. [1,2] where experimental data for the DSIFs and T-stress are available. Fig. 7 shows a schematic for free–free beams used in the test examples of this Section. Here, $L=200$ mm, $B=8.75$ mm (specimen thickness), $W=50$ mm, $e=0$ (mode I) or 25.4 mm (mixed mode), and crack length $a=10$ mm.

6.1. Numerical vs. experimental results for the DSIFs (mode-I case)

In this case, the beam is made from an epoxy prepared by mixing a bisphenol-A resin and an amine base hardner in the ratio 100:38 [1]. Young's modulus, Poisson's ratio, and the mass density of the cured material measured ultrasonically are $E=4.1$ GPa, $\upsilon=0.34$, and $\rho=1175$ kg/m^3, respectively [1]. The beam is subjected to an impact load P at the center of the top surface ($e=0$) with time history depicted in Fig. 6. A damping ratio $\zeta=0.5\%$ is employed for the numerical analysis [1]. For the case discussed herein, the time history before the crack initiation for the DSIFs is of interest.

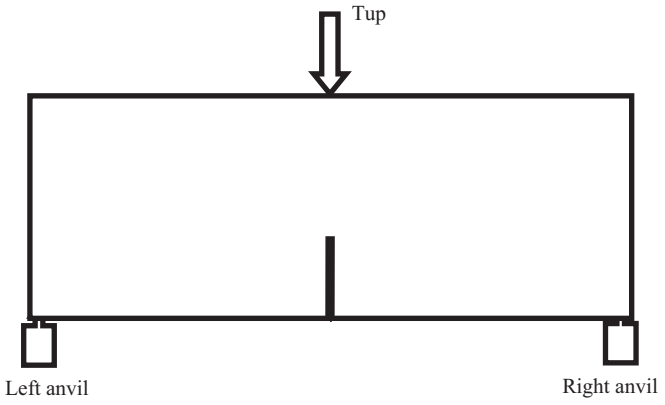

Fig. 5. Specimen configuration for mode-I dynamic fracture experiment.

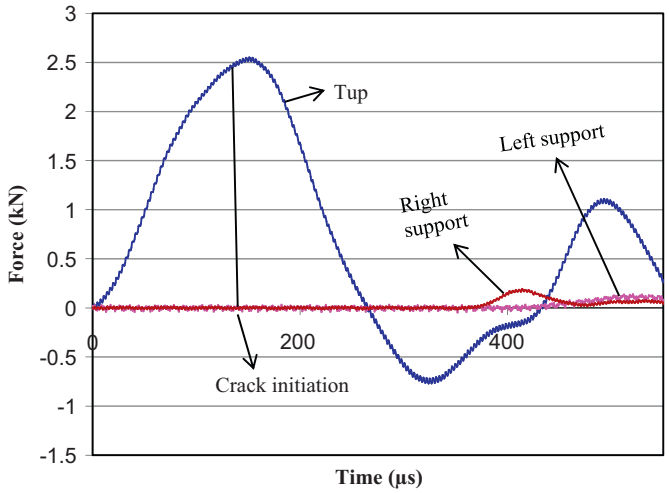

Fig. 6. Impact loading history for mode-I dynamic fracture experiment [1].

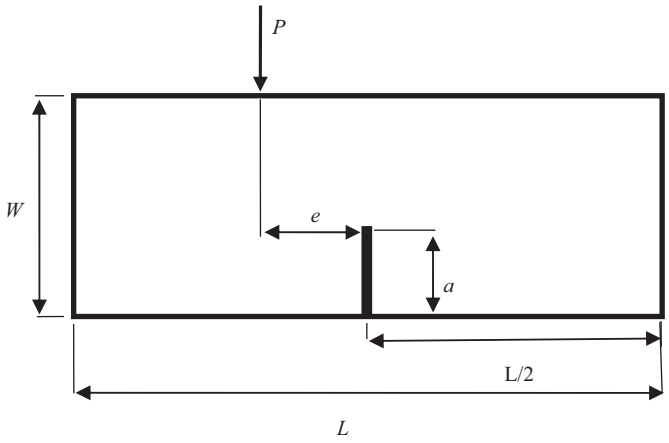

Fig. 7. Geometry and loading of the free–free beam model.

The frequency responses of the DSIFs are obtained using SGBEM with the following data: $\Delta f=25$ Hz, $N=2^{12}=4096$, $f_{Nyq}=51.2$ KHz. This results in the following values for the transient analysis using FFT and IFFT: $T_f=1/\Delta f=40$ ms and $\Delta t=T_f/N=9.766$ μs. In order to obtain accurate DISF results, a convergence test was carried out in which these results were plotted versus mesh refinement. This test suggests that a total of 65 elements for the boundary and 5 uniform elements for the crack are sufficient to achieve convergence, thus the accuracy of the SGBEM solution.

The SGBEM transient solution up to the crack initiation (at about 133 μs [1]) is shown in Fig. 8 together with the experimental and FEM results digitized from the related plot reported in Ref. [1]. Note in this case that the Nyquist frequency is doubled from 51.2 to 102.4 KHz to enhance the resolution of the SGBEM curves shown in Fig. 8. It can be seen from this figure that (a) the SGBEM solution for the mode-II DSIF (K_{II}) is zero as expected for this mode-I fracture case and (b) the SGBEM solution for K_I agrees very well with both the experimental and FEM results.

6.2. Numerical vs. experimental results for the DSIFs (mixed-mode case)

For this mixed-mode test, the beam is made from a syntactic foam prepared by a mixture of 25% of hollow micro glass spheres in a low-viscosity epoxy matrix. Young's modulus, Poisson's ratio,

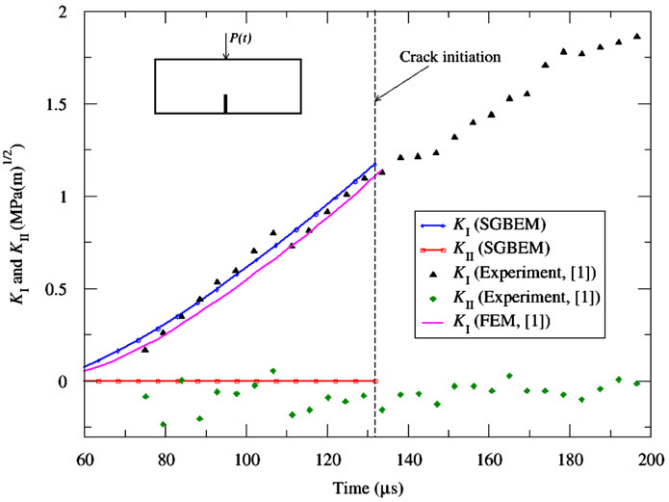

Fig. 8. Numerical vs. experimental solutions for the mode-I and -II DSIFs (mode-I case).

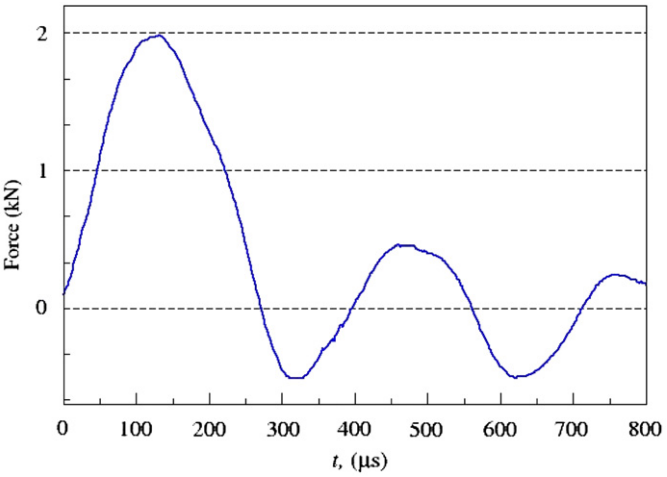

Fig. 9. Impact loading history for mixed mode case [2].

and the mass density of the cured material measured ultrasonically are $E=3.02$ GPa, $\upsilon=0.34$, and $\rho=870$ kg/m^3, respectively [2]. To create a mixed-mode fracture, the beam is subjected to an impact load P at a distance $e=25.4$ mm from center of the top surface of the beam. The time history of this load is depicted in Fig. 9 [2]. Again, a damping ratio $\zeta=0.5\%$ [2] is used for the dynamic analysis of the DSIFs for this case.

The same data as those reported in Section 6.1 are employed here to obtain the transient response of the mode-I and mode-II DSIFs (K_I and K_{II}) up to the crack initiation time (at about 175 μs [2]). These SGBEM solutions are compared with the experimental and FEM results as depicted in Fig. 10 where an excellent agreement can be seen.

6.3. Numerical vs. experimental results for the dynamic mode-mixity ψ (mixed-mode case)

The dynamic mode-mixity ψ is defined as the relative amount of in-plane shear stress to the normal shear stress. This parameter is related to the DSIFs as

$$\psi(t)=\tan^{-1}\left[\frac{K_{II}(t)}{K_I(t)}\right] \tag{27}$$

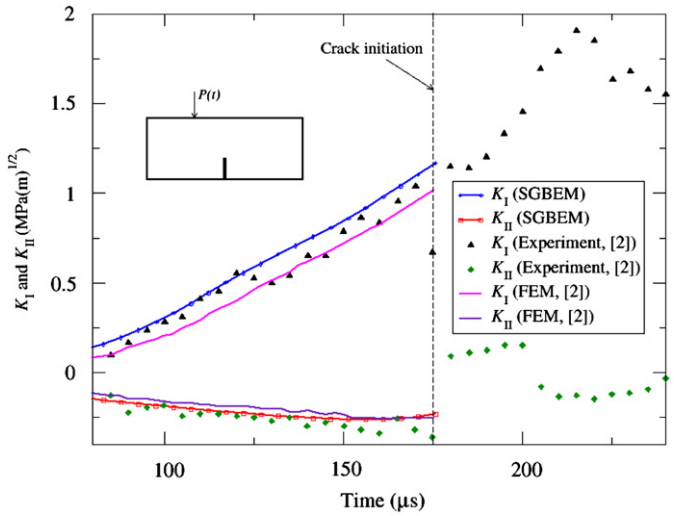

Fig. 10. Numerical vs. experimental solutions for the mode-I and -II DSIFs (mixed-mode case).

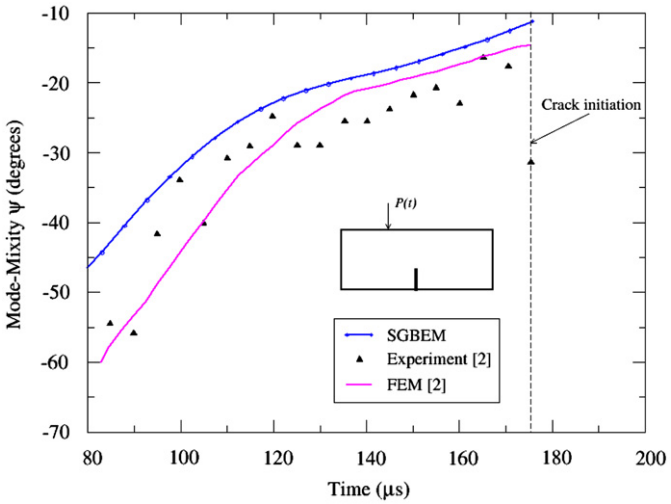

Fig. 11. Numerical vs. experimental solutions for the dynamic mode-mixity ψ.

This section is devoted to a comparison between the numerical and experimental solutions for the dynamic mode-mixity of the mixed-mode fracture case described in Section 6.2. Here, the SGBEM solution for the dynamic mode-mixity ψ is found by using the corresponding DSIF solution obtained in Section 6.2. As seen in Fig. 11, the SGBEM solution for ψ is favorably compared to the experimental and FEM results. Although the FEM solution appears to better match the experimental result than the SGBEM solution, any comment on the accuracy of the SGBEM solution should be inconclusive at this point as error estimates are unavailable for the experimental curve [2].

6.4. Numerical vs. experimental results for the dynamic biaxiality ratio β (mode-I case)

A dimensionless representation by the stress biaxiality ratio was first proposed by Leevers and Radon [33] as

$$\beta = T\sqrt{\pi a}/K_I \tag{28}$$

where a is the crack length.

For dynamic analysis of cracks, the same concept can be adopted to define the dynamic biaxiality ratio. Its time history is thus given by

$$\beta(t) = \frac{T(t)\sqrt{\pi a}}{K_I(t)} \tag{29}$$

As the dynamic biaxiality ratio is directly related to the DTS, this parameter is used in this section to assess the accuracy of the SGBEM solution for the DTS.

The mode-I fracture case of Section 6.1 is re-visited here. The SGBEM solution for the DTS for this problem is obtained using the technique discussed in Section 4. Again, the same data as reported in Section 6.1 are employed to obtain the transient response of the DTS. Finally, this DTS and the time history of the mode-I DSIF obtained in Section 6.1 are used in Eq. (29) to produce the transient response $\beta(t)$ up to the crack initiation (at about 133 μs) as shown in Fig. 12. The SGBEM solution can be seen to agree very well with the FEM solution while both these numerical solutions appear to be covered by the scattered data from the experimental measurement.

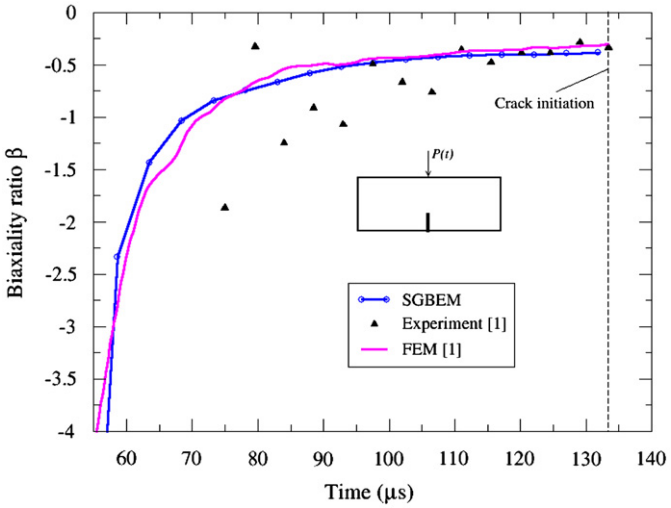

Fig. 12. Numerical vs. experimental results for the dynamic biaxiality ratio $\beta(t)$.

7. Conclusion

Transient analysis of the DISFs and DTS for some particulate composites, using the SGBEM for 2-D elastodynamics in the Fourier-space frequency-domain, in conjunction with the DCT (for the DSIFs) and SCT (for the DTS), is reported in this paper. To this end, effective material properties of particulate composites are required and they need to be measured experimentally or determined using micromechanics models. This transient analysis is performed for two fracture situations involving free–free beam models under mode-I and mixed-mode fracture. Here, frequency responses of the DSIFs and DTS are produced by the SGBEM. Subsequently, the FFT and IFFT are employed to convert the frequency-dependent solutions of these damped systems to time-dependent ones (transient responses or time histories). The two fracture cases are chosen from previous studies where experimental results are available. The motivation behind this work is to assess the accuracy of the SGBEM solutions via comparisons with experimental results rather than with those obtained from other numerical techniques. Four test examples, involving the mode-I DSIF, mixed-mode DSIFs, dynamic mode-mixity, and dynamic biaxiality ratio, are studied. Overall, the

SGBEM solutions agree very well with both the experimental and FEM solutions for all these examples. As excellent agreements have also been observed between the SGBEM solutions and those from other numerical methods such as FDM, BEM and SBFEM (see [16]), the numerical technique reported in this paper shows to be an effective tool for dynamic fracture analysis. Extending this technique to 2-D dynamic crack growth analysis is currently being pursued by the authors.

Acknowledgements

This research was supported in part by the NSF Grants CMMI-0653796 and CMMI-0653816, and the NASA Grant NNM07AA09A-03.

References

[1] Kirugulige MS, Tippur HV, Denney TS. Measurement of transient deformations using digital image correlation method and high-speed photography: Application to dynamic fracture. Applied Optics 2007;46:5083–96.
[2] Kirugulige MS, Tippur HV. Measurement of fracture parameters for a mixed-Mode crack driven by stress waves using image correlation technique and high-speed digital photography. Strain 2008;45:108–22.
[3] Dally JW. Dynamic photo-elastic studies of fracture. Experimental Mechanics 1979;19:349–61.
[4] Tippur HV, Krishnaswamy S, Rosakis AJ. Optical mapping of crack tip deformations using the methods of transmission and reflection coherent gradient sensing: a study of crack tip K-dominance. International Journal of Fracture 1991;52:91–117.
[5] Rousseau C-E, Tippur HV. Dynamic fracture of compositionally graded materials with cracks along the elastic gradient: experiments and analysis. Mechanics of Materials 2001;33:403–21.
[6] Kitey R, Tippur HV. Role of particle size and filler-matrix adhesion on dynamic fracture of glass-filled epoxy: I. macromeasurements. Acta Materialia 2005;53:1153–65.
[7] Kirugulige, MS, Tippur, HV. Mixed-mode dynamic crack growth in functionally graded glass-filled epoxy. Experimental Mechanics, 46, pp. 269–81.
[8] Kokaly MT, Lee J, Kobayashi AS. Moire interferometry for dynamic fracture study. Optics and Lasers in Engineering 2003;40:231–47.
[9] Jiang F, Rohatgi A, Vecchio KS, Cheney J. Analysis of the dynamic responses for a pre-cracked three-point bend specimen. International Journal of Fracture 2004;127:147–65.
[10] Ivanyts'kyi YaL, Boiko VM, Khodan IV, Shtayura ST. Stressed state of a cylinder with external circular crack under dynamic torsion. Materials Science 2007;43:203–14.
[11] Maleski MJ, Kirugulige MS, Tippur HV. A method for measuring mode I crack tip constraint under static and dynamic loading conditions. Experimental Mechanics 2004;44:522–32.
[12] Chen YM. Numerical computation of dynamic stress intensity factors by a Lagrangian finite difference method. Engineering Fracture Mechanics 1975;7:653–60.
[13] Song SH, Paulino GH. Dynamic stress intensity factors for homogeneous and smoothly heterogeneous materials using the interaction integral method. International Journal of Solids and Structures 2006;43:4830–66.
[14] Dominguez J. Boundary elements in dynamics. Southampton Boston: Computational Mechanics Publications; 1997.
[15] Phan A-V, Gray LJ, Salvadori A. Symmetric-Galerikin boundary element analysis of dynamic stress intensity factors in the frequency domain. Mechanics Research Communications 2010;37:177–83.
[16] Phan A-V, Gray LJ, Salvadori A. Transient analysis of the dynamic stress intensity factors using SGBEM for frequency-domain elastodynamics. Computer Methods in Applied Mechanics and Engineering, in press, doi:10.1016/j.cma.2010.06.019.
[17] Yang ZJ, Deeks AJ, Hao H. Transient dynamic fracture analysis using scaled boundary finite element method: a frequency-domain approach. Engineering Fracture Mechanics 2007;74:669–87.
[18] Aratollahi MR, Pavier MJ, Smith DJ. Determination of *t*-stress from finite element analysis for mode I and mixed mode I/II loading. International Journal of Fracture 1998;91:283–98.
[19] Yang B, Ravi-Chandar K. Evaluation of elastic *T*-stress by the stress difference method. Engineering Fracture Mechanics 1999;64:589–605.
[20] Sutradhar A, Paulino GH. Symmetric galerkin boundary element computation of *t*-stress and stress intensity factors for mixed-mode cracks by the interaction integral method. Engineering Analysis with Boundary Elements 2004;28:1335–50.
[21] Phan A-V. A non-singular boundary integral formula for determining the *T*-stress for cracks of arbitary geometry, submitted for publication.
[22] Song CM, Vrcelj Z. Evaluation of dynamic stress intensity factors and *t*-stress using the scaled boundary finite-element method. Engineering Fracture Mechanics 2008;75:1960–80.
[23] Phan A-V, Guduru V. Boundary element transient analysis of the dynamic *T*-stress and biaxiality ratio, Rivista di Matematica della Università di Parma, in press.
[24] Sladek J, Sladek V, Fedelinski P. Computation of the second fracture parameter in elastodynamics by the boundary element method. Advances in Engineering Software 1999;30:725–34.
[25] Sutradhar A, Paulino GH. Symmetric galerkin boundary element method. Berlin: Springer-Verlag; 2008.
[26] Bonnet M. Boundary integral equation methods for solids and fluids. England: John Wiley & Sons; 1995.
[27] Gray LJ, Phan A-V, Paulino GH, Kaplan T. Improved quarter-point crack tip element. Engineering Fracture Mechanics 2003;70:269–83.
[28] Aliabadi MH. The boundary element method: applications in solids and structures. England: John Wiley & Sons; 2002.
[29] Qu J, Cherkaoui M. Fundamentals of micromechanics of solids. New Jersey: John Wiley & Sons, Inc.; 2006.
[30] Wang, X. Elastic *T*-stress for cracks in test specimens subjected to non-uniform stress distributions. Acta Mechanica, 196, pp. 55–73.
[31] Williams ML. On the stress distribution at the base of a stationary crack. Applied Mechanics 1957;24:109–14.
[32] Brigham EO. The fast Fourier transform and its applications. New Jersey: Prentice Hall; 1998.
[33] Leevers PS, Radon JC. Inherent stress biaxiality in various fracture specimen geometries. International Journal of Fracture 1982;9:311–25.